Chalcogenide Letters Vol. 22, No. 11, November 2025, p. 971 - 985

Nanostructured Self-Organization of Lead Sulphide Quantum Dots by Electrophoretic Deposition (EPD) Technique

R. Yoga Indra Eniya, K. Vijayakumar and B. Vigneashwari*

PG & Research Department of Physics, Government Arts College for Men, Krishnagiri, 635001, Tamil Nadu, India
*Corresponding Author: B. Vigneashwari. Email: vigneashwari@gmail.com

Received: 11 November 2025; Accepted: 24 November 2025

ABSTRACT: Nanocrystals (~16 nm) of semiconducting lead sulphide (PbS) were synthesized using the co-precipitation method, which was characterized for phase and compositional purity. These ultrafine particles of PbS exhibited quantum confinement characteristics, which were revealed by blue-shifting in optical absorption using UV-DRS analysis. These QDs of PbS were driven under the influence of the applied electric field using monodispersed colloidal suspension on the Indium-Tin-Oxide (ITO) substrate using the electrophoretic deposition technique (EPD). The formation of self-organized arrays of PbS quantum dots (QDs) and their stacked assemblies was achieved through EPD. Interestingly, neither complexing agents nor templates were used for depositing PbS QDs. Also, the as-deposited film was not subjected to any post-heat treatment. EPD of PbS QDs emerges asa highly portable, cost-effective, short-duration, and pollution-free technique compared to all other known deposition methods. The crystallinity, size, morphology, and composition of PbS powder and film were characterized using PXRD, GIXRD, FESEM, SEM, and EDAX. The effect of controlling parameters such as distance between the electrodes, duration of deposition, and applied voltage was fixed as constant, and the obtained results were reported.

KEYWORDS: Lead sulphide; quantum dots; electrophoretic deposition; growth; self-organization

1 Introduction

In recent years, the colloidal chemistry methods have enabled the formation of monodisperse suspensions of quantum dots (QDs), which are fascinating building blocks for applications of photovoltaics, optoelectronics, bio-sensing, etc. [1–5]. For these fields of application, the assembly of individual QDs into larger structures, including monolayers, thin films, or super-crystals, is essential. Self-assembly of magnetic, metal-based, and semiconducting nanocrystals has been performed for making quantum dot superlattices [6–8]. The deposition of nanomaterials is crucial for their structural and chemical properties, which affect the particle size, morphology, shape, crystallinity, and dispersibility, where surface chemistry plays a pivotal role in achieving the desired performances of thin films, nanostructural coatings, and functional nanomaterials [9]. This could be accomplished by the different routes, which all have their particular strengths and weaknesses. Spin coating and drop casting methods permit the coverage of the substrate of quantum dot film, which ranges from sub-monolayer to micrometer thickness of the as-prepared deposits, where the films are not uniform [10,11]. Especially with the existence of charge-stabilized colloids, the electrophoretic deposition (EPD) method provides a substitute to prepare the nanostructure assemblies, which are suitable for full surface coverage [12], resulting in the outstanding quality of films with controlled thickness [13]. This EPD technique has a wide range of interests in both research and industrial sectors, not only due to its versatility but also because of its cost-effectiveness. It is an ancient method of deposition. Since 1808, Ruess, a Russian scientist, noticed the induced motion of clay particles in water under the influence of an applied electric field. The first practical application of EPD happened in 1933 for depositing the thoria particles on a platinum electrode, which was patented in the United States of America (USA). EPD is advantageous because of its simple apparatus, very few restrictions on the shape of the substrate, and mainly the short formation time.

The basic concept behind EPD is that the charged powder particles are suspended or dispersed in a liquid medium and are driven to be attracted and deposited on the surface of the conductive substrate of opposite charge when a DC electric field is applied. This technique offers advantages

https://doi.org/10.15251/CL.2025.2211.971

of easy control of morphology and thickness of the as-deposited film through minor adjustments of the applied potential and deposition time. EPD takes place when the DC electric field is applied perpendicular to the conductive substrate [12,13]. Also, a major difference between electrophoretic deposition (EPD) and electrolytic deposition (ELD) is that one is based on the suspension of particles in the solvent, and the other is based on the solution of salts of ionic species [14]. The necessary driving force for EPD is provided by the electrophoretic mobility and charge on the particles in the liquid media under the applied field. This technique has been successfully employed for high-T_c superconducting films, carbon nanotube (CNT) films, superconductors, piezoelectric materials, sensors, luminescent materials, and layered ceramics [15–23]. It is more important that the powdered particles should be completely dispersed and remain stable for smooth and homogenous deposition. For large-sized particles, the problem is that they tend to settle down because of gravity. EPD from the settled suspensions could result in a thicker deposit at the bottom and a thinner layer above the electrodes when it is placed vertically, but a uniform coating could not be obtained. EPD of large-sized particles occurs only with very strong surface charges. Additionally, the diameter of the particles < 1 μm or less tends to remain in the colloidal suspensions for a longer period because of Brownian motion, whereas particles with a diameter larger than 1 μm need ceaseless hydrodynamic agitation in order to persist in the colloidal suspension. Therefore, particle size has a prominent influence on the morphology and cracking of deposits [12]. Sato et.al [23] claimed that the reduction in particle size has improved the morphology of $YBa_2Cu_3O_{7-x}$ (YBCO) superconducting film assembled using EPD and suggest that this method is useful for minimizing the cracks on the films. The key parameters for the uniform EPD process are influenced by deposition time and applied voltage. Basu et al. investigated and reported that the rate of deposition for a constant electric field decreases with prolonged time of deposition. When the applied field is maintained between 25 and 100 V/cm, the film quality is more uniform, and if the applied field exceeds 100 V/cm, the film quality gets deteriorates [24]. Additionally, for the higher applied voltage, the particles move so fast that they may not find enough time to assemble in their best positions for the formation of a closely packed structure. It is quite important to understand the kinetics of EPD in order to obtain quality films, which depend on numerous parameters. It is beneficial to have a control of certain parameters during EPD because most of the parameters are inter-related to each other. The other research group reported that the quality of EPD films is heavily dependent on the suspension conditions [25]. It is obviously evident that the most dominating parameters of EPD process are deposition time, applied field (voltage), and concentration of particles in the suspension medium [26]. In EPD process, both direct current (DC) and alternating current (AC) power supply is used to generate an electric field but most commonly, the usage of DC power supply was reported by other research groups [12,27,28]. In general, it is preferred to utilize organic solvents for suspension medium because of the lower dielectric constant, which limits the charge on the particles. Because, the usage of water-suspensions for EPD could lead to electrolysis which could generate gas bubbles that could cause non-uniform deposited layers, which is considered to be the only drawback for the electrophoretic deposition technique [29].

Metal chalcogenides have gained the spotlight in the applications of materials science due to their unusual electronic characteristics and exotic chemical behaviors [30,31]. Semiconducting quantum dots manifest attractive features for the evolution of photovoltaic cells, overcoming the current limitations [32]. In recent years, a revolution in research has been leveled up due to the fascinating properties of materials in the quantum dots regime for their potential in device-based applications. The QDs offer intensified prospects in the optoelectronic materials because of the confinement phenomenon of phonons and charge carriers [33,34].

Lead sulphide (PbS), a IV-VI semiconducting compound with its small direct bandgap energy (0.41 eV), whereas the bandgap can be engineered in the wide range of 0.4 to 5.0 eV by size control, making it a promising material for optoelectronics such as LEDs, photodetectors, telecommunications, and photovoltaic devices [35–43]. PbS has larger excitonic Bohr radii of 18 nm, which allows strong quantum confinement of charge carriers. Since it is a narrow bandgap semiconductor, it has the potential to be relevant in long-wavelength imaging, diode lasers, and thermo-voltaic energy conversion **[44].** The primary strategies for PbS synthesis, which include

hydrothermal, reverse micelles, solvothermal routes, precipitation, sonochemical routes, etc., [45–51].

In this work, ultrafine crystalline particles of PbS were driven electrophoretically and deposited on a conductive substrate to form the nanocrystalline assemblies. This experiment was performed to investigate the assembly of nanostructures and their morphologies, which could provide insights about the kinetics of deposition parameters on the nature of assemblies, surface coverage, and quality of electrophoretically deposited PbS. Since there are only a few reports available on EPD of PbS QDs, which say that in order to achieve effective coating, deposition times of less than 2 h are required, but in other deposition techniques, several hours are needed. The utilization of PbS QDs in quantum-dot sensitized solar cells (QDSCs) means the properties could be tunable because of their enhanced light harvesting potential.

In this work we attempted EPD of PbS QDs, and the suitable suspension medium for deposition was chosen based on trial (such as toluene, isopropyl alcohol, etc., because, as per other research groups, there was difficulty in choosing a proper suspension medium for PbS because there were issues regarding the stability of the suspension. We analyzed the deposition of PbS QDs by maintaining the deposition time (t_d), applied voltage, and separation between the electrodes under the influence of a constant electric field.

2 Experimental Section

2.1 Synthesis of Lead Sulphide Nanoparticles

The co-precipitation method was employed to synthesize ultrafine particles of PbS. In this study, lead nitrate ($Pb(NO_3)_2$) and sodium sulphide (Na_2S) were purchased from the Aldrich company. To prepare the solutions, deionized water (DW) was used as the solvent. Initially, 1 M of $Pb(NO_3)_2$ and 0.5 M of Na_2S were dissolved individually in 40 mL of DW at the ambient temperature. The mixture was magnetically stirred for 3 h to ensure homogeneity. The formation of a greyish-black sol on constant stirring was observed. The obtained sol was centrifuged at 3000 rpm and continuously washed with DW and ethanol (Et-OH) to ensure purity of as-synthesized PbS. The resulting PbS powder was vacuum dried at 80°C for 2 h.

2.2 Electrophoretic Deposition (EPD) of Lead Sulphide

In this technique, the particles were suspended in a suitable medium since they possess a surface charge concerning the medium, which is transported by the application of an electric field towards a conductive substrate if the distance beyond which the interrelated electrostatic field decays is larger than that of the particle's size [52]. For EPD to take place, a DC power supply is used as the voltage source and an EPD cell comprises a counter electrode (stainless steel) and a working electrode. In this experiment, indium tin oxide (ITO-coated glass) is used as the working electrode, and a stainless-steel plate is used as the counter electrode. These two electrodes were separated using a spacer made of a Teflon block. To prevent impurities, the electrodes were washed using isopropyl alcohol (IPA) and acetone in an ultrasonic bath. The pair of electrodes was immersed into the EPD cell as presented in Fig. 1.

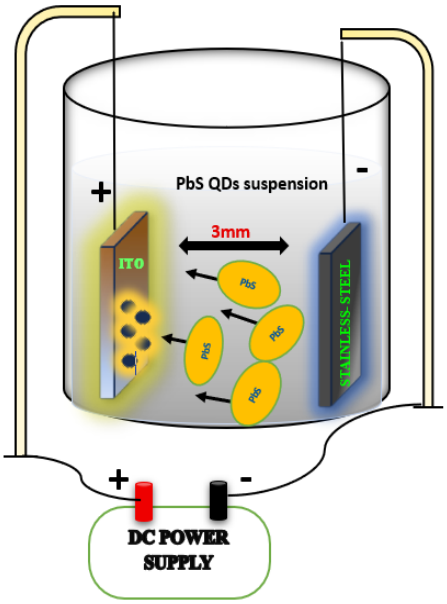

Figure 1: Schematic representation of the electrophoretic deposition (EPD) of PbS QDs.

To prepare the colloidal suspensions, 0.5 g of PbS ultrafine particles were suspended in 10 mL of pure acetone. In EPD, the suspension medium enables the charging of the EPD cell, where the particles acquire a surface charge and a DC voltage as a power supply for the transportation of surface charges between the electrodes. In order to avoid agglomeration and to uniformly disperse the individual grains, the suspension was prepared with the help of the ultrasonication process. The suspension was left to settle down for about 15 min, where the larger particles sedimented in the bottom of the beaker and smaller particles could be seen on top, as shown in Fig. 2.

Figure 2: Colloidal suspension of PbS QDs in pure acetone.

The decanted solution was carefully transferred into the EPD cell. Since the features of film could be controlled by modifying the influential parameters like electrode separation, deposition voltage, duration of deposition, and concentration of suspension. In this work we report that the distance between the electrodes was 3 mm, as displayed in Fig. 1, and the applied voltage (30 V) and the deposition time (t_d = 120 s) were fixed, and it is considered the most optimal condition for

EPD of PbS QDs, which was witnessed by complete discoloration of the colloidal QD solution. It could be understood that EPD is mainly governed by two phenomena: movement of charged particles (electrophoresis) and accumulation of particles on the conductive substrate (deposition). During this process, the solution containing charged colloidal PbS QDs were attracted towards the oppositely charged electrode (ITO). The coated substrate was carefully detached from the EPD cell. The obtained deposits were dried naturally at normal conditions.

3 Characterization Techniques

Powder X-ray diffraction (PXRD), Grazing incidence X-ray diffraction (GIXRD), Ultraviolet diffuse reflectance spectroscopy (UV-DRS) for PbS-powder, Scanning electron microscopy (SEM) was used for analysing the morphology of PbS powder and were used to study the assembly of as-deposited nanoclusters, and Energy dispersive X-ray analysis (EDAX) was used for compositional and elemental analysis before and after deposition.

4 Results and Discussion

4.1 Physical Characterization:

4.1.1 Powder X-ray Diffraction Analysis of PbS Powder

The PXRD profiles of as-synthesized PbS powder were performed using a Bruker AXS D2 phaser X-ray diffractometer with Cu-Kα radiation as the source, having a wavelength of 1.5406 Å. The GIXRD pattern of the as-deposited assembly was carried out using a Bruker D8 Advance with a scan rate of 2°/min, having an incidence angle of 0.5°. Fig. 3 shows the PXRD (a) and GIXRD (b) modes of powder and deposited samples, respectively. It suggests that both samples are relatively indexed to the face-centered cubic phase of PbS, where the obtained XRD profiles are well matched with the #JCPDS card no. 78-1900. The existence of a high intensity of (200) planes is observed in the powder sample, which suggests a strong preference for oriented crystal habit, which was absent in the case of the deposited film. The PXRD pattern of as-synthesized powder indicates good crystallinity and phase purity and is devoid of any secondary phases. The nanocrystalline nature of the as-prepared powder could be seen from the significant line broadening of the peak profiles.

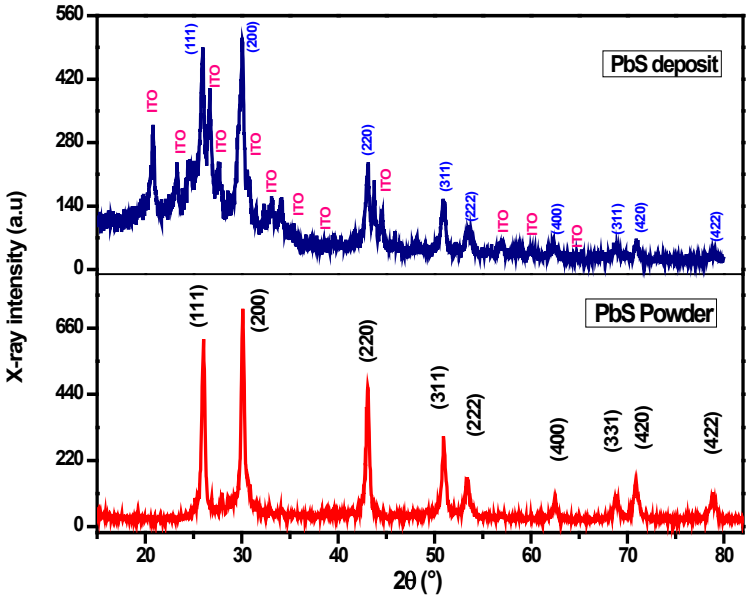

Figure 3: Comparison of PXRD and GIXRD patterns of PbS powder versus deposit.

Grazing incidence X-ray Diffraction Analysis of PbS Film

In the GIXRD pattern of PbS deposit, no other impurity peaks were noticed, but the signature peaks of ITO substrates were seen. The peak broadening in the diffraction pattern reveals that the as-deposited PbS retains the nanocrystalline nature. To calculate the crystallite size, Debye-

Scherrer's formula was used. The average crystallite size of the highest intensity peak corresponding to the (111) plane, the PbS powder, and the deposits was calculated as 16 nm and 12 nm, respectively.

Table 1: Comparison of 2θ values and variation of average crystallite size (D) for PbS powder and deposit.

Test Conditions	2θ Values	D(nm)
PbS-powder	26.03°	16 nm
	30.12°	
	43.07°	
	50.93°	
	53.41°	
	62.51°	
	68.82°	
	70.95°	
	78.87°	
PbS-deposits	ITO	12 nm
	ITO	
	26.01°	
	ITO	
	ITO	
	30.11°	
	43.06°	
	ITO	
	50.92°	
	53.40°	
	ITO	
	ITO	
	62.50°	
	ITO	
	68.81°	
	70.92°	
	78.85°	

The particles in the PbS deposits were found to have a smaller size, which is due to the settling down of bigger particles, where we have used only the decanted part of the suspension for deposition, because it contains only smaller particles. The intensity of diffraction peaks of the PbS deposits has been affected under the electric field, which indicates a reduction in crystallite size as compared to the powder. The broadening of diffraction peaks in the deposited film also indicates that the crystallite size is reduced during EPD. Additionally, there is a slight peak shift in 2θ values of PbS deposits was illustrated in Table 1, which is attributed to structural disorders in the deposited films. Such a shift in XRD peaks could be recognized because of lattice strain, which might be due to structural disorder generated during the film growth [53,54]. From the investigation of the structural properties of powder and deposited film, there were no signatures of phase transformation of PbS when driven with the help of applied voltage.

4.2 Optical Characterization of PbS Powder

The optical absorption spectrum of the lead sulphide powder was obtained using the Jasco-UV-Vis-NIR (V-770, Serial No. A012061801) spectrophotometer in the UV-Visible range. Fig. 4 represents the UV-DRS spectra of the PbS powder sample. The absorption edge was observed within 300 to 400 nm, and the onset wavelength was estimated to be 366 nm for PbS powder. This could be explained by the quantum-confined characteristics of the excitons because the size of lead sulphide nanocrystallites was comparable to the corresponding excitonic Bohr radius (r_B) [53]. The blue shift in the optical absorption spectrum as compared to that from the bulk PbS55,56] . A similar kind of blue-shift because of quantum confinement has been observed, and the additional reports of

such high band gap values attributed to the quantum confined transitions of PbS are available in the literature [57,58].].

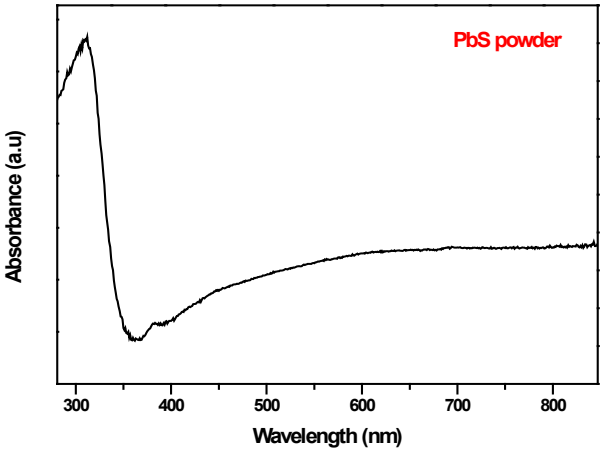

Figure 4: UV-DRS spectrum of PbS powder.

From the optical absorption spectrum of lead sulphide, the optical bandgap energy of PbS powder was calculated using the following relation [59] : $E_g = hc/\lambda$, where E_g represents the optical bandgap energy and λ is the absorption wavelength. The calculated optical bandgap was found to be 3.38 eV, which is larger than the bandgapenergy of bulk PbS (0.41 eV). Such an increase in the optical band gap energy indicates the as-prepared PbS powder is within the quantum dot regime, which could be further confirmed by detailed morphological analysis.

4.3 Morphological Analysis

For morphological characterization of Powder-PbS, field emission scanning electron microscopy (FESEM) was performed, using model Apreo 2s HiVac. From Fig. 5, it is evident that the morphology of the powder had very fine-sized rice-like grains with irregular shapes that were analyzed at lower and higher magnifications, which was also reported in [60]. On first sight of the FESEM image of the powder sample, it is clear that there are numerous numbers of particles that resemblethe accumulation of PbS quantum dots.

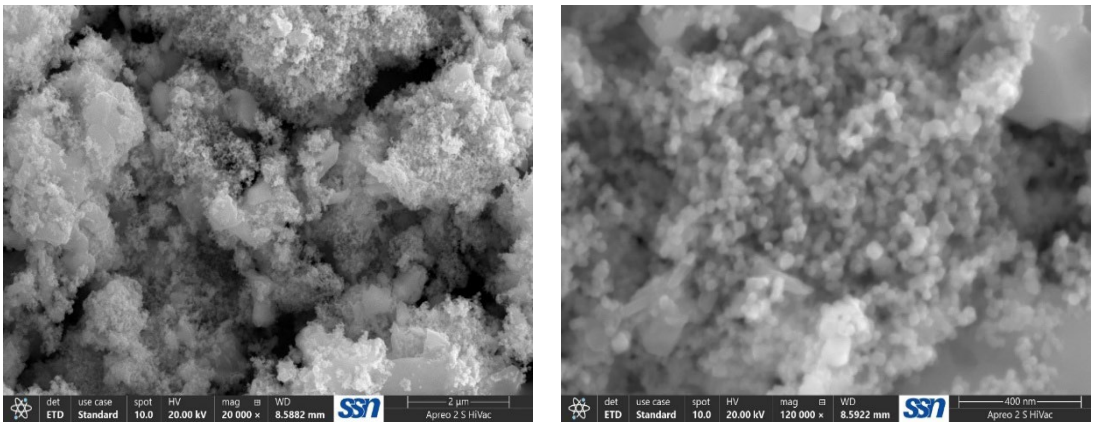

(a) **(b)**

Figure 5: FESEM images of PbS powder.

For better understanding of such microstructures, the average particle size was obtained using ImageJ software. Each rice-like grain has an average particle size of 33 nm, and the corresponding histogram of average particle size distribution is presented in Fig. 6. According to literature, the crystallite size and particle size are bound to one another [61]. The calculated particle size of PbS

powder was larger than the crystallite size obtained from Scherrer's equation in PXRD analysis. This is because each particle is made up of ultra-fine crystallites to form a PbS particle. The calculated average crystallite size of the PbS-powder sample was found to be 16 nm, which is quite smaller than the excitonic Bohr radius (r_B = 18 nm). After deposition of such PbS QDs using EPD, one could explore interesting features, which were discussed in detail.

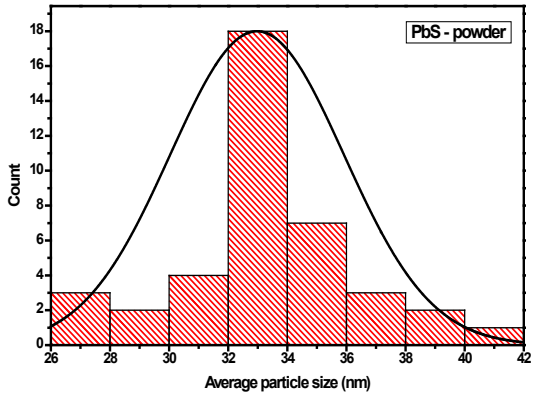

Figure 6: Particle size distribution of PbS-powder sample.

4.4 Compositional Analysis

PbS powder and deposit were characterized by EDAX coupled with SEM from Quorum Technologies, U.K., for investigating the compositional characteristics. The EDAX exhibits distinct peaks corresponding to lead (Pb) and sulphur presence in the PbS powder, which indicates that no other impurities existed during sample preparation, whereas for PbS deposits, the peaks related to the ITO substrate with the elements O, Si, Na, and In were identified. As shown in Fig. 7b, the characteristic peaks of Pb and S were indicated during analysis. The absence of additional peaks in the EDAX of PbS deposits confirms the formation of high-purity film.

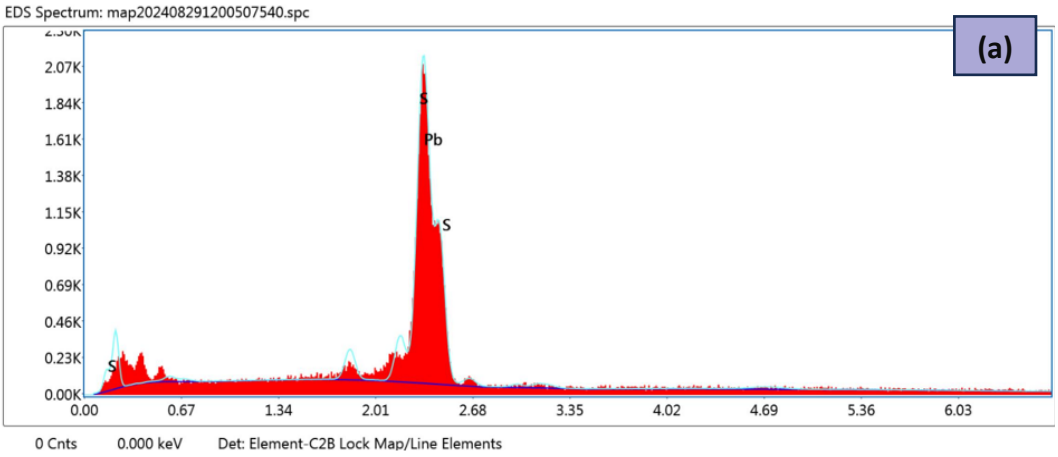

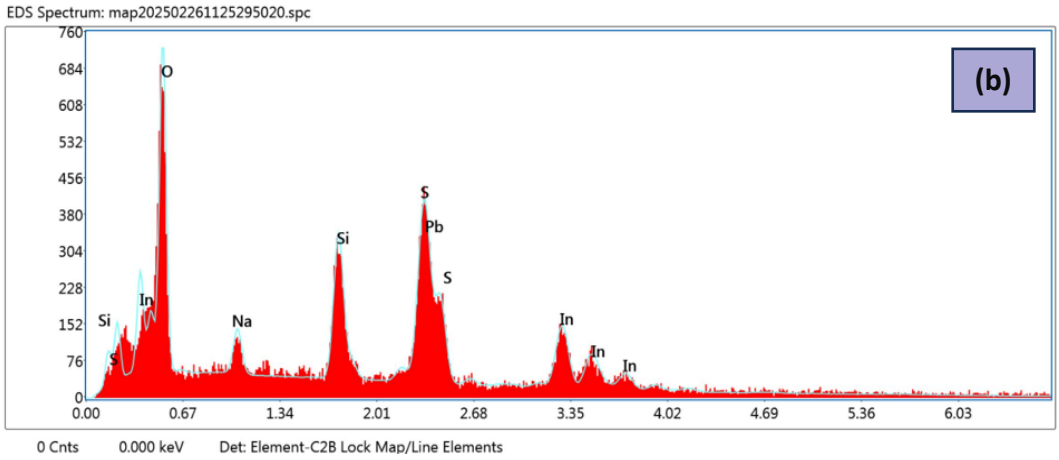

Figure 7: Compositional analysis by SEM/EDAX of PbS (**a**) powder (**b**) deposit.

4.5 Morphological Characterization of PbS Deposits

A Weswox optical microscope was used to primarily analyze the assembly of deposits at a magnification of 10×. Fig. 8 displays the optical micrograph of bare ITO and PbS deposits. The images were captured at the center of the as-deposited film to investigate the uniformity and information about the cracks and surface coverage in the PbS deposit. In this work, EPD was carried out at 30 V; it could be seen that the as-deposited film is crack-free, with maximum surface coverage achieved. It is more important to choose suitable liquid media for EPD; there should not be a chemical reaction with the dispersed particles, but it should be able to generate surface charge on the surface of the particles [62]. Also, the particles in PbS powder obtained surface charge in acetone medium without any additives or charge boosters. In this work, the obtained PbS films were allowed to dry naturally instead of using the sintering or fast evaporation method, and so the resulting deposits were crack-free during drying. Surprisingly, it is clear that the uniformity of film was achieved with EPD of PbS QDs, and traces of islands due to the influence of the applied electric field could be seen.

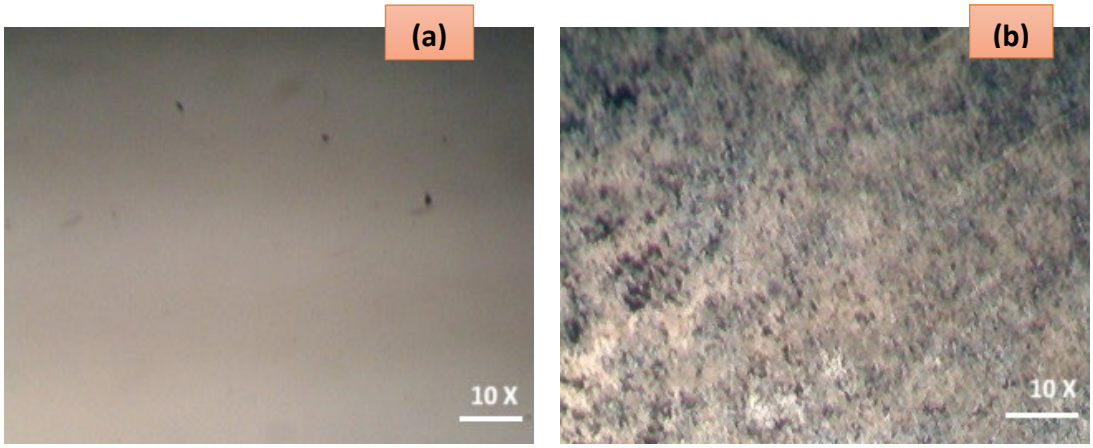

Figure 8: Optical microscope image of (**a**) bare ITO and (**b**) PbS deposit.

In order to investigate the details of structural assembly, surface coverage, and electrically driven PbS nanocrystallites, a scanning electron microscope was employed to maximize the morphological nature of as-deposited thin film. By using Carl Zeiss (Germany) Microscopy GmbH—Model No. EVO 18, SEM images were acquired at different locations of deposits. In Fig. 8a‑f, a set of SEM images of the PbS deposit at different magnifications are displayed.

To the best of our knowledge, there were no reports based on PbS QDs EPD with acetone as a suspending medium, and also, the particles were well dispersed and stable in the suspension because the nanocrystallites in the PbS powder were 16 nm, which was found to be less than the excitonic

Bohr radius (for PbS $r_B = 18$ nm). From fig. 9a, at the lower magnification, it is visible that the clusters of PbS QDs are evenly assembled. As seen in the optical microscope image, the duration of 120 s led to uniformity of the as-deposited film. The surface coverage has been achieved, and the resulting film is free from voids, which could happen if the duration of deposits exceeds. Also, in fig. 9b, the growth tendency of clusters led to the growth of an island (as marked in the circle), which was as similar as stated in [63]. To understand in detail about the formation of the island, the magnified image is presented in Fig. 9c. Interestingly, the organization of rice-like nanostructures that have grown perpendicular to the ITO substrate can be observed. Remarkably, rice-like nanostructures are embedded within the island, and the smaller-sized particles are assembled around them, which was presented in Fig. 9f. Comparing the FESEM image of PbS powder, the rice-like geometric arrangement was retained under EPD. Such an arrangement of self-organized fractal structures is the characteristic of quantum dot assemblies [53,64,65].

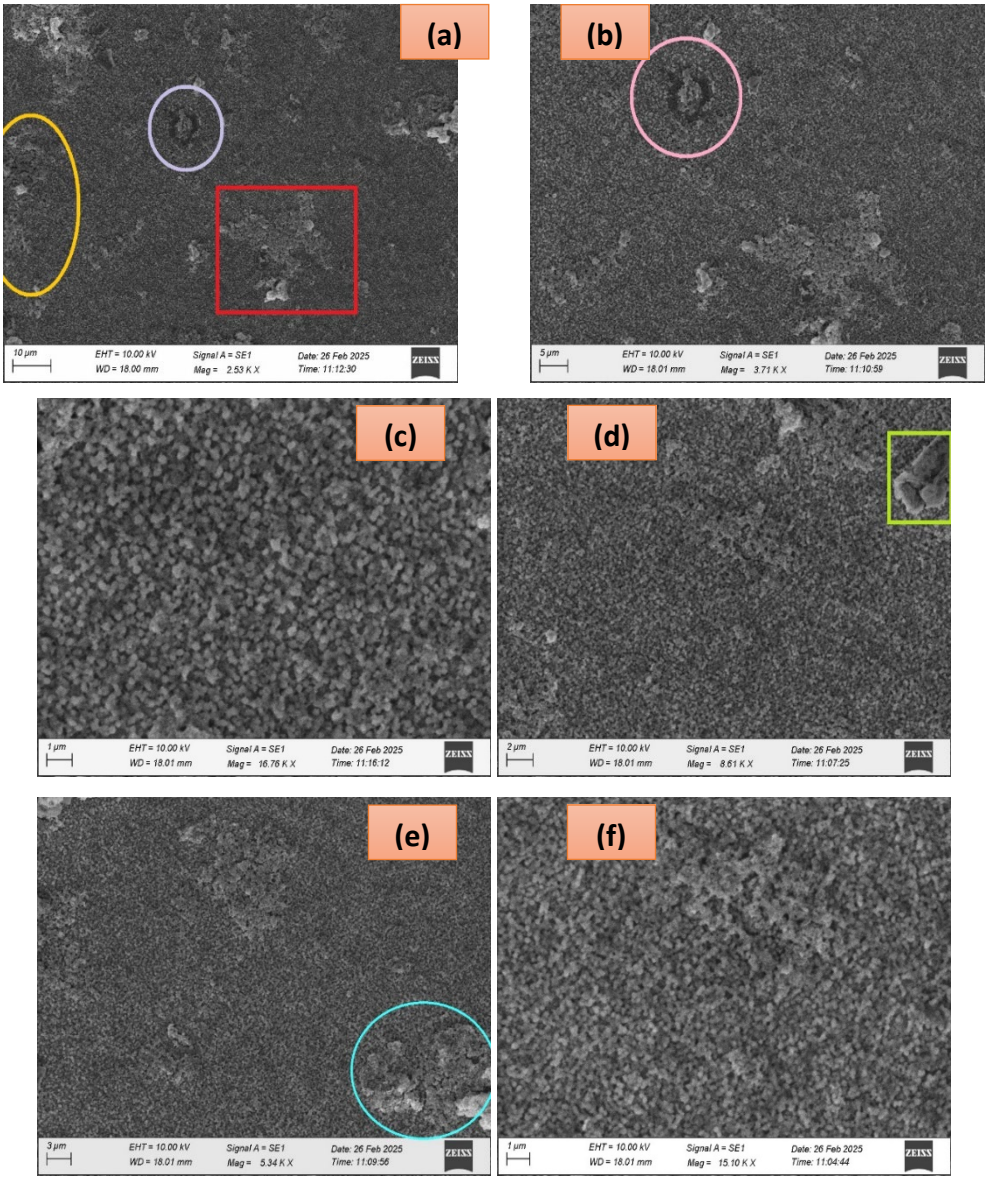

Figure 9: (**a**–**f**) SEM images of PbS deposit.

According to researchers [12], the particles with similar diameter tend to assemble themselves and get packed together and form the orderly packed area. The same analogy happened with the deposition of PbS QDs. The deposition voltage of 30 V and deposition duration of 120 s could be considered as the optimal conditions for EPD of PbS QDs, because it has good surface coverage,

but in some regions, there is a field-induced aggregation of PbS QDs, which led to deposition of larger aggregates seen in the higher magnification image (Fig. 9d). Similar kinds of fractal formations of CdSe QDs under the influence of an electric field by the electrophoretic deposition method were reported [66]. The growth of the second PbS QDs layer could be noticed after the completion of the first layer, where small 2D islands were formed on the first layer. This phenomenon of filling of the second layer is similar to the growth of the first one. This characteristic behavior is known as layer-by-layer or even termed as the Frank-Van der Merwe growth mechanism. By clearly looking into Fig. 9e, we see a network of thin chains that got merged during the formation of the 2nd layer (as marked in the blue-colored circle). In EPD of PbS QDs, aggregation of clusters was seen. As per literature [12], during the formation of clusters, it rapidly grows along the z-axis with respect to the plane of the film as shown in Fig. 10, and the distance above which they try to attract the newly arrived particle on the surface increases. According to Boehmer [67], particles that arrive at a cluster tend to move around its boundary until they reach their most favorable electrically driven position, i.e., the place where they may have been merged into the already prevailing lattice. Such kinds of ordered arrays of nanostructures in 2D configuration exhibit novel properties that are not attainable in individual particles.

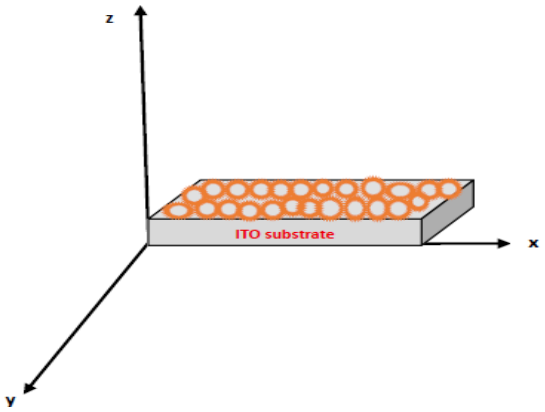

Figure 10: Representation of the growth of PbS deposits along the *z*-axis with respect to the plane of the film.

Overall SEM images of PbS deposits explain that EPD at 120 s, with 30 V, islands of nanostructures begin to form. Additionally, along with these islands, small clusters of nanostructures and individual nanoparticles were deposited on the surface of the electrode. It is significant to mention that the individual particles that existed in suspension used for EPD were only a few nanometers (nm) in size when deposited based on the interaction of the layer adjacent to the substrate and the particles assembled themselves and got deposited, which was driven by the applied electric field. The interaction energy between the dispersed particles could be explained by two mechanisms: Van der Waals and electrostatic forces [68]. Potential areas of applications include photovoltaic cells, antireflecting coatings, luminescent devices, sensors, diodes, optoelectronics, etc. Self-assembled nanostructures of PbS powder deposited using the EPD method will pave the way for utilizing EPD as an alternative and pollution-free route to deposit the self-organized deposition method of semiconductor QDs for photovoltaic applications and photodetectors. To understand more about the electrically driven ultrafine PbS QDs as self-organized deposits in certain island-like areas, the conductivity characterization is yet to be analyzed, and we are waiting for some interesting results.

5 Conclusion

In summary, quantum dots of lead sulphide, a semiconductor with its application in photovoltaics and optoelectronic devices, were synthesized and evaluated before using it for electrophoretic deposition using PXRD and FESEM analysis. Using EPD, PbS QDs were deposited and organized under the applied electric field, fixing the deposition parameters as constant. The obtained results in SEM suggest that deposition of PbS QDs is influenced by particle size and

concentration of suspension, which leads to the formation of islands and the growth of more ordered, stacked, self-organized arrays by the electrophoretic deposition method.

Moreover, comparison between PbS-film fabricated from PbS-powder played a vital role in charge formation during the EPD process and generated a uniform and crack-free deposit. Under the conditions of deposition parameters of 30 V, t_d = 120 s is characterized by a novel ring-shaped island where the ultrafine nanostructures were stacked, which were surrounded by clusters of PbS nanocrystallites. Hence, a smooth and uniform PbS film was obtained with the applied electric field strength and lower deposition time. In this work, EPD of PbS QDs, the charged particles, were spontaneously organized into self-assembled and more ordered rice-like structures. Such an assembly of self-organized nanostructured materials finds its applications in optoelectronics, energy storage devices and photovoltaics.

Acknowledgement: Not applicable.

Funding Statement: The author(s) recieved no specific funding from any agencies. The APC was funded by the author(s)

Author Contributions: R.Yoga Indra Eniya 1 - Data collection, draft manuscript preparation, K.Vijayakumar 2 -Formal analysis, B.Vigneashwari 3 – supervision, formal analysis. All the authors reviewed the results and approved the final version of the manuscript

Availability of Data and Materials: The authors confirm that the data supporting the findings of this study are available within this article.

Ethics Approval: Not applicable

Conflicts of Interest: The authors declare no conflicts of interest to report regarding the present study.

1. ReferencesAlivisatos A P, Gu W W and Larabell C, 2005 Annu. Rev. Biomed. Eng. 7 55-76
2. Brus L 1991 Appl. Phys. A 53, 465-74; https://doi.org/10.1007/BF00331535
3. Klimov V I, Mikhailovsky A A, Xu S, Malko A, Hollingsworth J A, Leatherdale C A, Eisler H J and Bawendi M G2000 Science 290 314-7.
4. Moreels I, Lambert K, De Muynck D, Vanhaecke K, Poelman D, Martins J C, Allan G, Hens Z 2007 Chem. Mater. 19, 6101-6; https://doi.org/10.1021/cm071410q
5. Gur I, Fromer N A, Geier M L, and Alivisatos A P 2005 Science 310 462-5.
6. C. B. Murray, C. R. Kagan, M. G. Bawendi, Science 270, 1335 (1995); https://doi.org/10.1126/science.270.5240.1335
7. C.P. Collier, R.J. Saykally, J.J. Shiang, S.E. Henrichs. R. Heath, Science 277, 1978 (1997); https://doi.org/10.1126/science.277.5334.1978
8. S. Sun, C. B. Murray, D. Weller, L. Folks, A. Moser, Science 287, 1989 (2000); https://doi.org/10.1126/science.287.5460.1989
9. Nanomaterials: a review of synthesis methods, properties, recent progress, and challenges - Materials Advances (RSC Publishing)
10. Mohammad A. Islama, Yuqi Xia, Benjamin J. Kraines, Irving P. Hermana, Mat. Res. Soc. Symp. Proc. Vol. 737 © 2003 Materials Research Society.
11. PLommens, D VanThourhout, P F Smet, D Poelman, Z Hens, Nanotechnology 19 (2008),245301, (6pp); https://doi.org/10.1088/0957-4484/19/24/245301
12. Besra L, Liu M, 2007, Prog. Mater. Sci. 52, 1-61; https://doi.org/10.1016/j.pmatsci.2006.07.001
13. M.A. Islam, I.P. Herman, Appl. Phys. Lett. 80, 3823 (2002); https://doi.org/10.1063/1.1480878
14. Zhitomirsky I., Adv Colloid Interface Sci 2002;97:279-317; https://doi.org/10.1016/S0001-8686(01)00068-9
15. Ochsenkuehn-Petropoulou MT, Altzoumailis AF, Argyropoulou R, Ochsenkuehn KM. Superconducting coatings of MgB2 prepared by electrophoretic deposition. Anal Bioanal Chem 2004;379:792-5; https://doi.org/10.1007/s00216-004-2668-0
16. Sarka P, Mathur S, Nicholson PS, Stager CV, J Appl Phys 1991;69(3):1775-7; https://doi.org/10.1063/1.347230
17. Du C, Heldbrant D, Pan N., Mater Lett 2002;57:434-8; https://doi.org/10.1016/S0167-577X(02)00806-6
18. Maiti HS, Datta S, Basu RN., J Am Ceram Soc 1989;72(9):1733-5; https://doi.org/10.1111/j.1151-2916.1989.tb06314.x
19. Yau SKF, Sorrel CC., Physica C 1997;282-287:2563-4; https://doi.org/10.1016/S0921-4534(97)01378-6
20. Van Tassel J, Randall CA., J Eur Ceram Soc 1999;19:955-8; https://doi.org/10.1016/S0955-2219(98)00352-5
21. Hayashi K, Furuya N., J Electrochem Soc 2004;151(3):A354-7; https://doi.org/10.1149/1.1641034
22. Dougami N, Takada T., Sens Actuators B 2003;93:316-20; https://doi.org/10.1016/S0925-4005(03)00219-3
23. Ferrari B, Sanchez-Herencia AJ, Moreno R., Mater Res Bull 1998;33(3):487-99; https://doi.org/10.1016/S0025-5408(97)00244-4
24. Basu RN, Randall CA, MayoMJ., J Am Ceram Soc 2001;84(1):33-40; https://doi.org/10.1111/j.1151-2916.2001.tb00604.x

25. Ma J, Chen W., Mater Lett 2002;56:721-7; https://doi.org/10.1016/S0167-577X(02)00602-X
26. Vandeperre L, Van Der Biest O, Clegg WJ., Key Eng Mater (Pt. 1, Ceramic and Metal Matrix Composites) 1997;127-131: 567-73; https://doi.org/10.4028/www.scientific.net/KEM.127-131.567
27. Yoshioka T, Chávez-Valdez A, Roether J, Schubert D, Boccaccini A (2013), J Colloid Interface Sci 392:167-171; https://doi.org/10.1016/j.jcis.2012.09.087
28. Gardeshzadeh A, Raissi B, Marzbanrad E (2008), Mater Lett 62(10-11):1697-1699; https://doi.org/10.1016/j.matlet.2007.09.062
29. Pouya Amrollahi, Jerzy S. Krasinski, Ranji Vaidyanathan, Lobat Tayebi, Daryoosh Vashaee, Handbook of Nanoelectrochemistry.
30. H. Anders, G. Michael, Chem. Rev, 95. 49 (1995); https://doi.org/10.1021/cr00033a003
31. W.S. Sheldrick, M. Wachhold, Angew. Chem. Int. Ed., 36, 207, (1997); https://doi.org/10.1002/anie.199702061
32. A.J. Nozik, Physica E, 2002, 14, 112-200; https://doi.org/10.1046/j.0021-8782.2001.00010.x
33. L.E. Brus, J. Phys. Chem. 90,2555 (1986); https://doi.org/10.1021/j100403a003
34. Y. Wang, N. Herron, J.Phys. Chem. 95, 525, (1991); https://doi.org/10.1021/j100155a009
35. R. Thielsch, T. Bohne, R. Reiche, D. Schlafer, H.D. Bauer, H. Bottcher, Nanostruct. Mater. 10 (1998) 131; https://doi.org/10.1016/S0965-9773(98)00056-7
36. J.S. Steckel, S. Coe-Sullivan, V. Bulovic, M.G. Bawendi, Adv. Mater. 15 (2003) 1862; https://doi.org/10.1002/adma.200305449
37. A.L. Rogach, N. Gaponik, J.M. Lupton, C. Bertoni, D. Gallardo, D. Dunn, N. Pira, M. Paderi, P. Reppeto, S. Romanov, C.O.' Dwyer, C. Sotomayo, A. Eych muller, Angew. Chem. Int. Edn. 47 (2008) 6538; https://doi.org/10.1002/anie.200705109
38. H. Eisler, V.C. Sundar, M.G. Bawendi, M. Walsh, H.L. Smith, V. Klimov, Appl. Phys. Lett. 80 (2002) 4614; https://doi.org/10.1063/1.1485125
39. G. Konstantatos, I. Howard, A. Fischer, S. Hoogland, J. Clifford, E. Klem, L. Levina, E.H. Sargent, Nature 442 (2006) 180; https://doi.org/10.1038/nature04855
40. S. Mc Donald, G. Konstantatos, Shiguo Zhang, P. Cyr, E. Klem, L. Levina, H. Sargent, Nat. Mater. 4 (2005) 138; https://doi.org/10.1038/nmat1299
41. X. Jiang, R.D. Schaller, S.B. Lee, J.M. Pietryga, V.I. Klimov, Anvar A. Zakhidov, Mater. Res. 22 (2007) 2204; https://doi.org/10.1557/jmr.2007.0289
42. A.S. Obaid, M.A. Mahadi, Z. Hassan, Optoelectron. Adv. Mat. **6**, 422 (2012)
43. A. Stavrinadis, A. Rath, F. Pelayo, S.I. Diedenhofen, C. Magen, L. Martinez, D. So, G. Konstantatod, Nat. Commun. 4 (2013) 2981; https://doi.org/10.1038/ncomms3981
44. R. Palomino Merino, O. Portillo Moreno, J.C. Flores Gracia, J. Hernandez Tecorralco, J. Martinez Juarez, A. Moran Torres, E. Rubio Rosas, G. Hrenandez Tellez, R. Gutierrez, L.A. Chaltel Lima, J. Nanoci. Nanotech. 14 (2014) 5408e5414; https://doi.org/10.1166/jnn.2014.8664
45. M. Shakouri-Arani, M. Salavati-Niasari, J. Ind. Eng. Chem. (2014), Vol. 20,(5), 3141-3149, https://doi.org/10.1016/j.jiec.2013.11.057
46. Khiew, P.S.; Radiman,S.; Huang, N.M.; Ahmad, M. S., J. Cryst. Growth.2003, 254, 235; https://doi.org/10.1016/S0022-0248(03)01175-8
47. Wang, D.; Yu, D.; Shao, M.; Liu X.; Yu, W.; Qian, Y., Cryst. Growth Des. 2003, 257, 384; https://doi.org/10.1016/S0022-0248(03)01470-2
48. Ni, Y.; Liu, H.; Wang, F.; Liang, Y.; Hong, J.; Ma, X.; Xu, Z. Cryst. Res. Technol. 2004, 39, 200; https://doi.org/10.1002/crat.200310171
49. S. Jana, S. Goswami, S. Nandy, K.K. Chattopadhyay, J. Alloys Compd. 481, 806-810 (2009); https://doi.org/10.1016/j.jallcom.2009.03.110

50. H. Karami, M. Ghasemi, S. Matini, Int. J. Electrochem. Sci. 8, 11661-11679 (2013); https://doi.org/10.1016/S1452-3981(23)13213-5
51. Anukorn Phuruangrat, Somchai Thongtem, Titipun Thongtem, Budsabong Kuntalue, Digest Journal of Nanomaterials and Biostructures Vol. 7, No. 4, October-December 2012, p. 1413-1417.
52. Vigneashwari B, Ravichandran V, Parameswaran P, Dash S, Tyagi AK., J Nanosci Nanotechnol. 2008 Feb;8(2):689-94; https://doi.org/10.1166/jnn.2008.A128
53. Nima Parsi Benehkohal, Victoria González-Pedro, Pablo P. Boix, Sudam Chavhan, Ramón Tena-Zaera, George P. Demopoulos, Iván Mora-Seró, J. Phys. Chem. C 2012, 116, 31, 16391-16397; https://doi.org/10.1021/jp3056009
54. P.Prathap, N.Revathi, Y.P.Venkata, Subbaiah K. T. and Ramakrishna Reddy, J. Phys. Condens. Matter. 20 035205; https://doi.org/10.1088/0953-8984/20/03/035205
55. [56] Shkir. M, Chadekar. K.V., Alshahrani. T. et al., Journal of materials research 35, 2664-675 (2020).
56. Oviya Sekar, F.IRine Maira Bincy, Raju Suresh Kumar, Kannappan Perumal, Ikhyun Kim, S.A.Martin Britto Dhas, Dalton Trans., 2025; https://doi.org/10.1039/D4DT03393K
57. S. Obregón, G. Amor, A. Vázquez, Advances in Colloid and Interface Science 269, 236 (2019); https://doi.org/10.1016/j.cis.2019.05.003
58. Černohorský O, Grym J, Yatskiv R, Pham VH, Dickerson JH., ACS Appl Mater Interfaces. 2016 Aug 3;8(30):19680-90; https://doi.org/10.1021/acsami.6b04746
59. A. Böker, Y. Lin, K. Chiapperini, R. Horowitz, M. Thompson, V. Carreon, T. Xu, C. Abetz, H. Skaff, A. D. Dinsmore, T. Emrick, T. P. Russell, Nature Mat. 3, 302 (2004); https://doi.org/10.1038/nmat1110
60. B. Vigneashwari, P. Kanimozhi, V. Narayanan, S. Dash, A. K. Tyagi, T. R. Ravindran, V. Ravichandran, Synth. React. Inorg. Met. Org. Chem. 36, 209 (2006); https://doi.org/10.1080/15533170500524694
61. B. Vigneashwari, S. V. M. Satyanarayana, International Journal of Nanoscience Vol. 10, No. 6 (2011), 1215-1223; https://doi.org/10.1142/S0219581X11008198
62. Boehmer M., Langmuir 1996;12(4):5747-50; https://doi.org/10.1021/la960183w
63. P. Sarkar, D. De, T. Uchikochi, L. Besra, Electrophoretic deposition of Nanomaterials, pages 181-215, Springer (2011); https://doi.org/10.1007/978-1-4419-9730-2_5
64. Zamin Q. Mamiyev, Narmina O. Balayeva, Optical Materials, Volume 46, August 2015, Pages 522-525; https://doi.org/10.1016/j.optmat.2015.05.017
65. Sreekumar R, Jayakrishnan R, Sudha Kartha C, Vijayakumar KP, Khan SA, Avasthi DK (2008). J Appl Phys 103(2):023709-023719; https://doi.org/10.1063/1.2829812
66. X. Liu, M. Zhang, Int. J. Infrared. Millim. 21, 1697 (2000); https://doi.org/10.1023/A:1006676029014
67. F.G. Hone, F.B. Dejene, J. Lumin. 201, 321 (2018); https://doi.org/10.1016/j.jlumin.2018.05.004
68. Vijayakumar, K., Eniya, R. Y. I., Vigneashwari, B. (2025), Asian Journal of Chemistry, 37(7), 1743-1752; https://doi.org/10.14233/ajchem.2025.33974